Reflection Analysis of FDTD Boundary Conditions—Part II: Berenger's PML Absorbing Layers

Deane T. Prescott, *Member, IEEE,* and Nicholas V. Shuley, *Member, IEEE*

***Abstract*— This paper presents an in-depth analysis of Berenger's perfectly matched layer (PML) boundary truncation technique. The impedance and dispersion relationships for the fields within the PML media are derived to gain a better understanding of the nature of field propagation within such regions. The mechanisms which contribute toward reflection from a PML region are then described. Using this knowledge of the PML absorbing layers, a numerical method is developed, which allows the reflection from such layers to be calculated exactly.**

***Index Terms*— Absorbing boundary conditions, FDTD, time domain.**

I. Introduction

RECENTLY, Berenger [1] introduced the perfectly matched layer (PML) as an alternative to the conventional absorbing boundary conditions to truncate the computational domain in finite-difference time-domain (FDTD) simulations. The novelty and efficiency of this technique has created a large amount of interest and is set to revolutionize the FDTD field.

The more commonly used absorbing boundary conditions, such as that proposed by Mur [2], calculate the FDTD boundary fields as a function of the internal FDTD fields, their time history, and a knowledge of the outgoing wave's propagation characteristics. These methods unfortunately have been shown in the past to be very sensitive to the frequency and propagation direction of the radiation incident upon them [3]. As a result, these boundaries have had to be placed at large distances from radiators and scatterers, such that they can be effective.

The PML truncation technique operates in a completely different manner. Instead of approximating the outward traveling radiation, a layer of absorbing material is placed around the outer boundaries of the FDTD computational domain. Outward traveling waves then gradually diminish as they travel deeper into the lossy material, effectively being absorbed. This layer also has the property that it is *perfectly matched*. The wave impedance in the PML is the same as the space which it surrounds, which results in a theoretically reflectionless transmission of all waves into the PML medium. The reflection from a PML boundary is then dependant only upon the PML's depth and conductivity, and is independent of frequency and incidence angle. A PML boundary, designed to give a required level of absorption, can then be placed extremely close to any scatterer/radiator.

A number of authors [4], [5], have already made use of PML boundaries, managing to obtain extraordinarily low levels of reflection. Katz *et al*. [6] extended the PML technique to three-dimensional (3-D) space, and Jurgens [5] implemented PML boundaries in cylindrical coordinates. Gribbons, Pinello, and Cangellaris [7] investigated the impact of PML's on the dispersive characteristics of planar waveguiding structures.

To date, however, there exists little comment within the literature upon the mechanisms behind the reflection from PML layers, methods to calculate such reflections without performing an FDTD simulation, and more importantly, how to design PML layers. The object of this contribution is to rigorously analyze wave propagation within the PML medium such that the reflection from a PML boundary can be computed exactly. It is hoped that this will then be the first step toward designing the most efficient PML boundaries possible.

The methodology behind the PML boundary will be briefly described first. The dispersion relationship for the fields within the PML media will then be derived so that one has an exact knowledge of the relationships between the nodal fields in both space and time. Next, it will be shown that the wave impedance is indeed *perfectly matched*—this will aid in the understanding of wave transmission from free-space into a PML medium. The various mechanisms which contribute toward producing reflections will be described and how the total reflection from an arbitrary PML boundary can be calculated will be demonstrated. Finally, some numerical results based upon the authors' findings will be provided.

II. Theory

A. The PML Absorbing Boundary Method

This section briefly describes the theory behind the PML absorbing boundary method. For greater detail, the reader is referred to [1] and [6]. The theory will be presented and analyzed in two-dimensional (2-D) space using the x–z plane. We will be concerned only with the H_x, H_z, E_y

Manuscript received October 17, 1995; revised April 25, 1997.

D. T. Prescott was with the Department of Electrical and Computer Engineering, The University of Queensland, Qld., Q4072, Australia. He is now with the Australian Defense Science and Technology Organization (DSTO), Salisbury, S.A. 5108, Australia.

N. V. Shuley is with The University of Queensland, Qld., Q4072, Australia. Publisher Item Identifier S 0018-9480(97)05370-2.

field components (TM^y polarization). However, the theory is applicable for 2-D TE and 3-D FDTD PML.

The PML is an artificial lossy medium. It is characterized by an electrical conductivity σ and a magnetic conductivity σ^*. These are chosen to give a required level of attenuation within the medium and are related to each other as follows:

$$\frac{\sigma}{\epsilon_0} = \frac{\sigma^*}{\mu_0}. \tag{1}$$

This relationship ensures that the wave impedance inside the PML equals the free-space wave impedance, and that the phase velocity inside the PML is the vacuum speed of light [6].

Berenger also shows that transmission through PML/PML interfaces of any arbitrary incident wave will be reflectionless if the conductivity has a certain anisotropy characteristic. For this, Berenger demonstrates that the components of the conductivities in the direction(s) transverse to, and either side of, the media interface must be equal. Now since free-space can be considered as a PML region with $\sigma_x = \sigma_y = \sigma_z = 0$, then the tangential to the boundary components of the conductivities in a PML region should be set to zero. Excluding corner regions, which will not be discussed in this paper, this implies that the PML medium has only a normal (to the boundary) directed component of conductivity.

Consider a PML half-space, located at $z \geq 0$ (see Fig. 1). The PML/PML matching condition described above will result in the conductivity being anisotropic with only σ_z being nonzero. To deal with this anisotropy, the FDTD equation for the E_y field component, which involves differentials in both the x- and z-directions, must be split into two subcomponents, E_{yx} and E_{yz}. This results in there being four coupled field equations for the PML region as follows:

$$\epsilon_0 \frac{\partial E_{yx}}{\partial t} = -\frac{\partial H_z}{\partial x} \tag{2}$$

$$\epsilon_0 \frac{\partial E_{yz}}{\partial t} + \sigma_z E_{yz} = \frac{\partial H_x}{\partial z} \tag{3}$$

$$\mu_0 \frac{\partial H_x}{\partial t} + \sigma_z^* H_x = \frac{\partial (E_{yx} + E_{yz})}{\partial z} \tag{4}$$

$$\mu_0 \frac{\partial H_z}{\partial t} = -\frac{\partial (E_{yx} + E_{yz})}{\partial x}. \tag{5}$$

These equations can be descretized to form the FDTD time-stepping equations for the PML region. The field equations which do not contain a conductivity component, (2) and (5), are discretized in exactly the same way as the equivalent standard-FDTD equations. For the remaining field equations (3) and (4), explicit exponentially differenced time-stepping is employed [1], [8]. The resulting four FDTD time-stepping equations for the PML region are then

$$E_{yx}^{n+1}(i,k) = E_{yx}^{n}(i,k) - \frac{\Delta t}{\epsilon_0 \Delta x} \cdot [H_z^{n+1/2}(i+\tfrac{1}{2},k) - H_z^{n+1/2}(i-\tfrac{1}{2},k)] \tag{6}$$

$$E_{yz}^{n+1}(i,k) = e^{-\sigma_z(k)\Delta t/\epsilon_0} E_{yz}^{n}(i,k) + \frac{1 - e^{-\sigma_z(k)\Delta t/\epsilon_0}}{\sigma_z(k)\Delta z} \cdot [H_x^{n+1/2}(i,k+\tfrac{1}{2}) - H_x^{n+1/2}(i,k-\tfrac{1}{2})]p \tag{7}$$

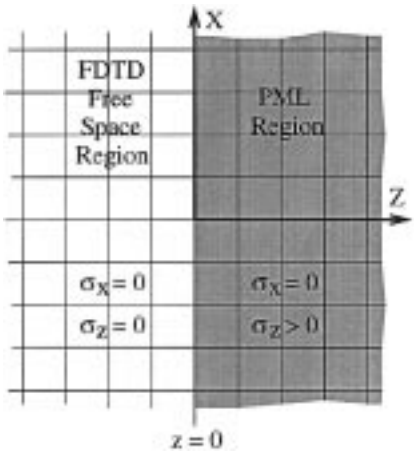

Fig. 1. A PML/free-space boundary in the x–z plane.

$$H_x^{n+1/2}(i,k+\tfrac{1}{2}) = e^{-\sigma_z^*(k+1/2)\Delta t/\mu_0} H_x^{n-1/2}(i,k+\tfrac{1}{2}) + \frac{1 - e^{-\sigma_z^*(k+1/2)\Delta t/\mu_0}}{\sigma_z^*(k+\tfrac{1}{2})\Delta z} [E_{yx}^{n}(i,k+1) + E_{yz}^{n}(i,k+1) - E_{yx}^{n}(i,k) - E_{yz}^{n}(i,k)] \tag{8}$$

$$H_z^{n+1/2}(i+\tfrac{1}{2},k) = H_z^{n-1/2}\left(i+\frac{1}{2},k\right) - \frac{\Delta t}{\mu_0 \Delta x} \cdot [E_{yx}^{n}(i+1,k) + E_{yz}^{n}(i+1,k) - E_{yx}^{n}(i,k) - E_{yz}^{n}(i,k)] \tag{9}$$

where Δx, Δz, Δt, n, i, and k have their usual FDTD meanings.

These equations can be directly implemented to model a PML medium in an FDTD simulation. All that is required is to choose the depth of the PML boundary and its conductivity. Theoretically, the PML boundary could be designed one Yee-cell deep and have near-infinite conductivity to produce maximum absorption. Unfortunately, reflections occur as a result of sharp variations in the conductivity. It has been shown that increasing the conductivity gradually with depth reduces the magnitude of these reflections; hence, the "layering" of the medium, $\sigma_z(k)$. It should also be noted that the PML region is usually terminated with an electric wall—however, this is not a necessary restriction.

B. Dispersion within the PML Medium

Before the reflection from the PML can be calculated, it is necessary for one to have a complete knowledge of exactly how the fields within the medium are related to each other and how they propagate. This is achieved by calculating the impedance and dispersion relationships for the PML medium.

A difference equation will first be derived involving only one field component for a homogenous PML region. From this, one will be able to obtain the dispersion relationship. We will solve for $E_y = E_{yx} + E_{yz}$ by solving for both E_{yx} and E_{yz} individually as functions of E_y, and then combining the results.

First, let one find $E_{yx}^{n+1} - E_{yx}^{n}$ by applying (6) twice in time. Thus

$$\begin{aligned} &E_{yx}^{n+1}(i,k) - E_{yx}^{n}(i,k) \\ &\quad = E_{yx}^{n}(i,k) - E_{yx}^{n-1}(i,k) - \frac{\Delta t}{\epsilon_0 \Delta x} \\ &\qquad \cdot [H_z^{n+1/2}(i+\tfrac{1}{2},k) - H_z^{n-1/2}(i+\tfrac{1}{2},k) \\ &\qquad - H_z^{n+1/2}(i-\tfrac{1}{2},k) + H_z^{n-1/2}(i-\tfrac{1}{2},k)]. \end{aligned} \tag{10}$$

If (9) is substituted into (10) and rearranged, then

$$\begin{aligned} &E_{yx}^{n+1}(i,k) - 2E_{yx}^{n}(i,k) + E_{yx}^{n-1}(i,k) \\ &\quad = \left(\frac{c\Delta t}{\Delta x}\right)^2 [E_y^n(i+1,k) - 2E_y^n(i,k) + E_y^n(i-1,k)] \end{aligned} \tag{11}$$

is obtained, where $c = 1/\sqrt{\mu_0 \epsilon_0}$ is the speed of light in a vacuum. To simplify the following section of this analysis the following substitution will be made:

$$\begin{aligned} A &= e^{-\sigma_z \Delta t/\epsilon_0} \\ &= e^{-\sigma_z^* \Delta t/\mu_0}. \end{aligned} \tag{12}$$

Now $E_{yz}^{n+1} - AE_{yz}^{n}$ can be found by applying (7) twice in time. Thus

$$\begin{aligned} &E_{yz}^{n+1}(i,k) - AE_{yz}^{n}(i,k) \\ &\quad = AE_{yz}^{n}(i,k) - A^2 E_{yz}^{n-1}(i,k) + \frac{1-A}{\sigma_z \Delta z} \\ &\qquad \cdot [H_x^{n+1/2}(i,k+\tfrac{1}{2}) - AH_x^{n-1/2}(i,k+\tfrac{1}{2}) \\ &\qquad - H_x^{n+1/2}(i,k-\tfrac{1}{2}) + AH_x^{n-1/2}(i,k-\tfrac{1}{2})]. \end{aligned} \tag{13}$$

If (8) is substituted into (13) and rearranged, then

$$\begin{aligned} &E_{yz}^{n+1}(i,k) - 2AE_{yz}^{n}(i,k) + A^2 E_{yz}^{n-1}(i,k) \\ &\quad = \left(\frac{1-A}{Z\sigma_z \Delta z}\right)^2 [E_y^n(i,k+1) - 2E_y^n(i,k) + E_y^n(i,k-1)] \end{aligned} \tag{14}$$

is obtained, where $Z = \sqrt{\mu_0/\epsilon_0}$ is the impedance of free-space.

Now, let one assume an $e^{j\omega t}e^{-jk_x x}e^{-jk_z z}$ dependence for all field components, where k_x and k_z are the wavenumbers in the x- and z-directions, respectively. At this point, one should note that k_z is now complex with the imaginary component indicating decay in the z-direction. If one substitutes this dependence into (11) and (14), then

$$\begin{aligned} &E_{yx}^{n}(i,k)[e^{j\omega\Delta t} - 2 + e^{-j\omega\Delta t}] \\ &\quad = E_y^n(i,k)\left(\frac{c\Delta t}{\Delta x}\right)^2 [e^{jk_x\Delta x} - 2 + e^{-jk_x\Delta x}] \end{aligned} \tag{15}$$

$$\begin{aligned} &E_{yz}^{n}(i,k)[e^{j\omega\Delta t} - 2A + A^2 e^{-j\omega\Delta t}] \\ &\quad = E_y^n(i,k)\left(\frac{1-A}{Z\sigma_z \Delta z}\right)^2 [e^{jk_z\Delta z} - 2 + e^{-jk_z\Delta z}] \end{aligned} \tag{16}$$

is obtained. By adding (15) to (16), one can form a single equation for $E_y^n(i,k)$—this is the dispersion relationship. With some algebra, one obtains

$$\begin{aligned} &\left(\frac{1}{c\Delta t}\right)^2 \sin^2\left(\frac{\omega\Delta t}{2}\right) \\ &\quad = \left(\frac{1}{\Delta x}\right)^2 \sin^2\left(\frac{k_x\Delta x}{2}\right) + \left(\frac{1}{\Delta z}\right)^2 \sin^2\left(\frac{k_z\Delta z}{2}\right) \times P^2 \end{aligned} \tag{17}$$

where

$$P = \frac{\epsilon_0(1-A)}{\sigma_z \Delta t} \frac{e^{j\omega\Delta t/2} - e^{-j\omega\Delta t/2}}{e^{j\omega\Delta t/2} - Ae^{-j\omega\Delta t/2}}. \tag{18}$$

Note that this field-dispersion relation differs from that for free-space in an FDTD domain [9] only by the multiplication of the z-dependent term by P^2, a factor which corrects for the effects of the PML conductivity. It can easily be shown that $P \to 1$ as $\sigma_z \to 0$, a result that would be expected.

Equation (17) can now be used to solve for k_z, which will be required when solving for the reflection from a PML medium.

C. Impedance of the PML Medium

The impedance of the PML medium can be defined in various ways. Since the impedance represents the ratio between the electric and magnetic fields, two impedances will be defined for the fields within a PML or FDTD region. These are

$$Z_x = \frac{E_y}{H_x} \tag{19}$$

$$Z_z = \frac{E_y}{H_z}. \tag{20}$$

To derive Z_z, one will substitute the harmonic dependance ($e^{j\omega t}e^{-jk_x x}e^{-jk_z z}$) into (9), thus

$$\begin{aligned} &H_z^n(i+\tfrac{1}{2},k)(e^{j\omega\Delta t/2} - e^{-j\omega\Delta t/2}) \\ &\quad = -E_y^n\left(i+\frac{1}{2},k\right)\frac{\Delta t}{\mu_0 \Delta x} \cdot (e^{-jk_x\Delta x/2} - e^{+jk_x\Delta x/2}). \end{aligned} \tag{21}$$

One can then find Z_z as

$$Z_z = \frac{\mu_0 \Delta x}{\Delta t} \frac{\sin\left(\frac{\omega\Delta t}{2}\right)}{\sin\left(\frac{k_x\Delta x}{2}\right)}. \tag{22}$$

It is easy to show that this is exactly the same as that for an FDTD region. In the case of Z_x, a little extra work is required. If the above procedure is repeated by substituting the harmonic dependence into (8), one obtains

$$Z_x = \frac{\mu_0 \sigma_z \Delta z}{\epsilon_0 (1-A)} \frac{e^{j\omega\Delta t/2} - Ae^{-j\omega\Delta t/2}}{e^{-jk_{zp}\Delta z/2} - e^{jk_{zp}\Delta z/2}} \tag{23}$$

where k_{zp} is the z-component of the wavenumber in the PML region. At this point, it appears as though this relationship is not the same as that for free-space. However, assume that the fields within the PML region are part of a plane wave that has travelled from free-space into the PML. It can be observed from the FDTD and PML time-stepping equations that the field dependance in the transverse (to the boundary) directions for

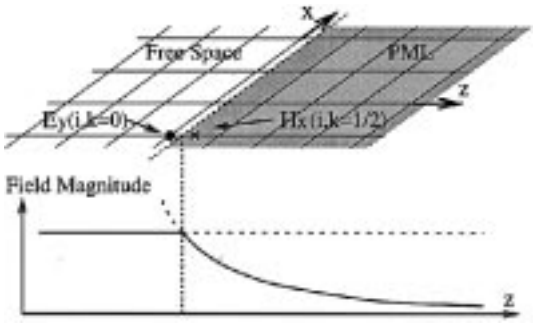

Fig. 2. Field components near a PML/free-space boundary.

the plane wave in both regions are identical—thus, $k_{xf} = k_{xp}$. If the dispersion relations for both regions are then compared, making note of the observation for k_x, then the following result can be deduced:

$$\frac{\epsilon_0(1-A)}{\sigma_z \Delta t} \frac{e^{j\omega\Delta t/2} - e^{-j\omega\Delta t/2}}{e^{j\omega\Delta t/2} - Ae^{-j\omega\Delta t/2}} \frac{e^{jk_{zp}\Delta z/2} - e^{-jk_{zp}\Delta z/2}}{e^{jk_{zf}\Delta z/2} - e^{-jk_{zf}\Delta z/2}} = 1 \tag{24}$$

where k_{zf} is the z-component of the wavenumber in the FDTD free-space region. If this result is substituted into (23), one obtains the same E_y, H_x impedance ratio Z_x that would be obtained for a free-space FDTD region

$$Z_x = -\frac{\mu_0 \Delta z}{\Delta t} \frac{\sin\left(\frac{\omega\Delta t}{2}\right)}{\sin\left(\frac{k_{zf}\Delta z}{2}\right)}. \tag{25}$$

The above results clearly show that Berenger's assumptions regarding the *perfect matching* of the PML region to FDTD free-space are correct.

D. Reflection from the PML Boundary

It can now be seen from the previous results that the PML medium has the same impedance as the FDTD medium which it encloses, and by solution of (17), one can readily find that any wave entering the PML region must decay as it travels deeper into the medium. Why then is there reflection from a PML absorbing boundary?

There are two mechanisms which govern the amount of reflection created by a PML absorbing boundary. These are: 1) reflections between PML/free-space and PML/PML interfaces and 2) the amount of decay experienced as the incident wave travels through the PML medium.

Reflections between the PML/free-space and PML/PML boundaries are the greatest contributor to the overall reflection. What creates these if the two regions are matched? Consider the field components on and near a PML/free-space boundary as shown in Fig. 2.

The field components on the free-space side are calculated using the FDTD time-stepping equations, whereas, the fields within the PML region are calculated using the PML exponentially differenced time-stepping equations (6)–(9). When calculating $E_y(i, k = 0)$ (Fig. 2) the FDTD equations require

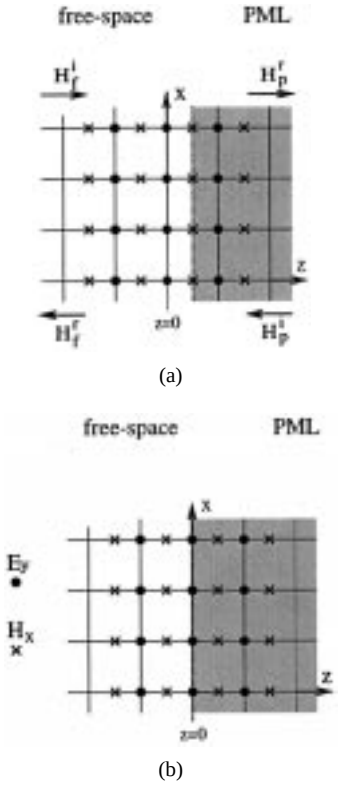

Fig. 3. Positioning of the PML/free-space boundary within the FDTD mesh (a) on the H_x field components and (b) on the E_y field components.

the magnitude of the field component $H_x(i, k = \frac{1}{2})$. If there is no reflecting wave, then the FDTD equation will expect the magnitude of $H_x(i, k = \frac{1}{2})$ to equal $E_y(i, k = 0)/Z_x$ (dotted line in Fig. 2). Unfortunately, because the $H_x(i, k = \frac{1}{2})$ field component is within the PML region, a small amount of decay has occurred to the $+z$ traveling wave, and the magnitude of this component is less than what the FDTD equations would expect. This results in the generation of the reflected wave.

In much the same way, the calculation of the $H_x(i, k = \frac{1}{2})$ field component using the PML equations would expect the magnitude of the $E_y(i, k = 0)$ component in the FDTD free-space region to be greater than what it would actually be.

So, to calculate the amount of reflection from the PML/free-space boundary, one must consider the fields calculated by both of the mismatched time-stepping equations.

Consider a PML/free-space boundary located at $z = \frac{1}{2}\Delta z$, [Fig. 3(a)], where the H_x field component is located on the boundary and is calculated as part of the PML region. At $z = \frac{1}{2}\Delta z$, the reflected and transmitted H_x field components on either side of the boundary must be matched. Thus

$$H_f^i + H_f^r = H_p^r + H_p^i \tag{26}$$

where H_f^i and H_f^r are the components of the H_x field, which are incident and reflecting (transmitting) from this node on the FDTD free-space side. H_p^i and H_p^r are the incident and reflecting (transmitting) components from the PML region as shown in Fig. 3(a).

At $z = 0$, the E_y component is calculated, and so the reflected and transmitted components here must be matched.

Thus

$$E_f^i + E_f^r = E_p^r + E_p^i. \tag{27}$$

Now these E_y field components are related to the H_x field components of (26) by the impedance Z_x and the spatial phase change which they undergo $e^{\pm jk_z\Delta z}$. Thus, (27) can be rewritten as

$$H_f^i e^{+jk_{zf}\Delta z/2} - H_f^r e^{-jk_{zf}\Delta z/2} = H_p^r e^{+jk_{zp}\Delta z/2} - H_p^i e^{-jk_{zp}\Delta z/2} \tag{28}$$

where k_{zf} and k_{zp} are the z-components of the wavenumber in the FDTD and PML regions, respectively.

Now the incident and reflected components on the PML side H_p^i and H_p^r are also related to each other by the reflection of the $+z$ traveling component, H_p^r, reflecting off the next boundary. Thus

$$H_p^i = H_p^r e^{-jk_{zp}2d} R^{H+} \tag{29}$$

where d is the distance to the next discontinuity and R^{H+} is the reflection experienced by an H_x field component at that discontinuity.

These three equations for the H_x field, (26), (28), and (29), can now be solved to find the total reflection $R^H_{H\,\mathrm{node}}$ for the H_x field at the free-space/PML boundary located at $z = \frac{1}{2}\Delta z$. Thus, $R^H_{H\,\mathrm{node}}$ is shown in (30) at the bottom of the page. However, there are some points to note about this result. This equation only applies to the calculation of the reflection for an H_x field component with the boundary placed upon a line of H_x nodes. The reflection for the E_y component at this H_x node is $R^E_{H\,\mathrm{node}} = -R^H_{H\,\mathrm{node}}$. If the free-space/PML boundary was located half a space step in the $\pm z$ direction, then one would have an E_y field component on the PML boundary and an H_x field component on the free-space FDTD side of the boundary [see Fig. 3(b)]. In this case, it can be shown by a very similar analysis that the reflection for an H_x field component from this boundary is $R^H_{E\,\mathrm{node}}$, shown in (31) at the bottom of the page. The total reflection from an arbitrary multilayered PML absorbing boundary can now be calculated simply by cascading the calculations for the reflections, interface by interface, from the perfect conductor at the edge of the PML layers back toward the FDTD free-space.

III. Numerical Results

The accuracy of the above technique for calculating the reflection from an arbitrary PML was checked using an FDTD simulator. However, the magnitude of the reflections in the FDTD simulations, which were performed at a single frequency, quickly converged upon those achieved using the analytical formulation. This occurred for all angles of incidence, frequency, and choice of PML construction. The FDTD simulation was found to agree with the analytical solution to an accuracy of around 10^{-8} of the magnitude of the monochromatic excitation. As a result, it is not feasible to compare the two methods for calculating the reflection graphically. The object of providing the numerical results contained in this section is to demonstrate the advantages of being able to accurately predict the reflective properties of a PML absorbing boundary. This analytical ability may then provide one with a greater insight into how the most suitable PML layering for a given problem is designed.

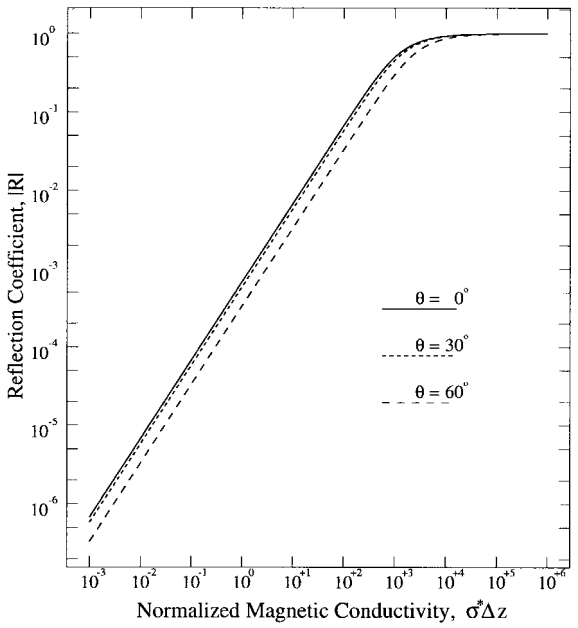

Fig. 4. Reflection from a PML/free-space boundary as a function of the normalized magnetic conductivity, $\sigma^*\Delta z$. $\lambda/\Delta z = 20$, (a) incidence angle $\theta = 0^\circ$, (b) $\theta = 30^\circ$, and (c) $\theta = 60^\circ$.

In the following sets of results, the conductivity and wavelength will be presented in a normalized form: $\sigma^*\Delta z$ and $\lambda/\Delta z$, respectively. One should, in fact, normalize with respect to Δt; however, since $\Delta x = \Delta z$ has been set, then Δt will be directly proportional to Δz. The reason for this normalization is that the spatial discretization size can then be neglected as a factor which may affect the amount of reflection from a PML boundary. It is also useful to use the $\lambda/\Delta z$ form, as this is also used as a criterion by which the FDTD-mesh discretization sizes are chosen.

The reflection resulting from a plane wave incident upon a PML half-space from a vacuum will be investigated first. This is performed by setting R^{H+} to zero in (30). Fig. 4 shows the reflection from a free-space/PML boundary as a

$$R^H_{H\,\mathrm{node}} = -\frac{e^{+jk_{zp}\Delta z/2} - e^{+jk_{zf}\Delta z/2} - R^{H+}e^{-jk_{zp}\Delta z/2} - R^{H+}e^{+jk_{zf}\Delta z/2}}{e^{+jk_{zp}\Delta z/2} + e^{-jk_{zf}\Delta z/2} - R^{H+}e^{-jk_{zp}\Delta z/2} + R^{H+}e^{-jk_{zf}\Delta z/2}} \tag{30}$$

$$R^H_{E\,\mathrm{node}} = \frac{e^{+jk_{zp}\Delta z/2} - e^{+jk_{zf}\Delta z/2} + R^{H+}e^{-jk_{zp}\Delta z/2} + R^{H+}e^{+jk_{zf}\Delta z/2}}{e^{+jk_{zp}\Delta z/2} + e^{-jk_{zf}\Delta z/2} + R^{H+}e^{-jk_{zp}\Delta z/2} - R^{H+}e^{-jk_{zf}\Delta z/2}} \tag{31}$$

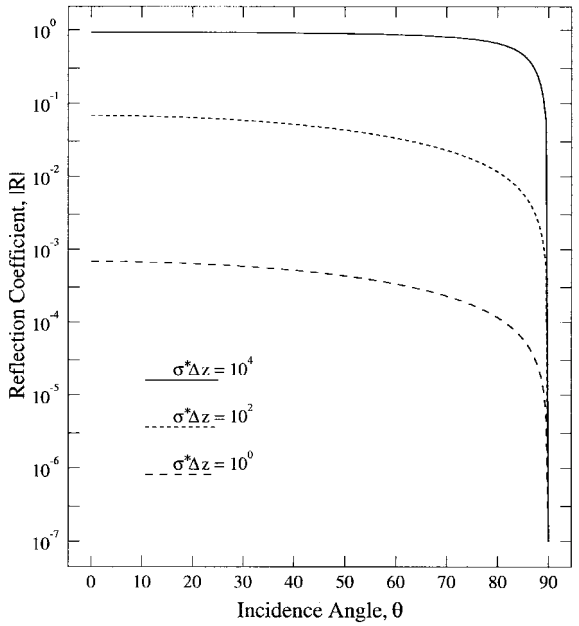

Fig. 5. Reflection from a PML/free-space boundary as a function of incidence angle θ. $\lambda/\Delta z = 20$. (a) $\sigma^*\Delta z = 10^0$, (b) $\sigma^*\Delta z = 10^2$, and (c) $\sigma^*\Delta z = 10^4$.

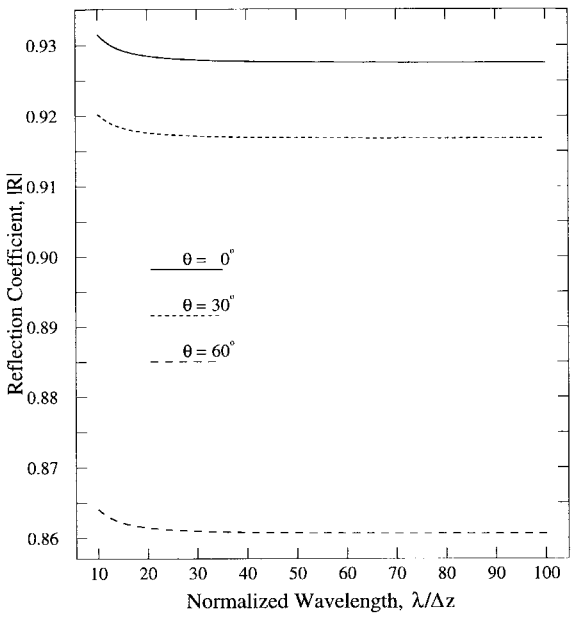

Fig. 6. Reflection from a PML/free-space boundary as a function of normalized wavelength, $\lambda/\Delta z$. $\sigma^*\Delta z = 10^4$. (a) incidence angle $\theta = 0°$, (b) $\theta = 30°$, and (c) $\theta = 60°$.

function of the normalized magnetic conductivity. One can see that as the conductivity is increased, so too does the amount of reflection. In fact, the increase is almost linear until approximately $\sigma^*\Delta z \approx 10^3$. At this point, the PML begins to act like a perfect conductor with the incident field being totally reflected.

It is also interesting to note that as the angle of incidence is increased, the amount of reflection decreases. In fact, one can see by examining (30) that if the incidence angle is increased to 90° then the reflection will decrease to zero. This effect can be readily seen in Fig. 5. It is interesting to note that the amount of reflection remains reasonably constant as the angle of incidence is increased until approximately $\theta \approx 70°$ when a severe drop off is experienced.

Fig. 6 demonstrates the dependence of the reflection upon the excitation wavelength. One can see that above $\lambda/\Delta z \approx 20$, the reflection becomes very constant.

Next, various PML constructions will be analyzed. Berenger examined a number of different forms of PML layering. In those cases, the conductivity was either constant or gradually increased from zero to a maximum σ_m at the electric-wall termination

$$\sigma(k) = \sigma_m \left(\frac{z}{d}\right)^n \tag{32}$$

where z is the depth within the PML region of total depth d, and n is the order of the conductivity's increase ($n = 1$ linear, $n = 2$ parabolic). Fig. 7 shows the effect of increasing the order of the polynomial, which governs the PML conductivity (32) upon the reflection as a function of the maximum conductivity.

One can readily see that introducing the conductivity gradually with depth does present improved performance over having a constant PML loss ($n = 0$). One can also note that increasing the order of the polynomial, which defines the

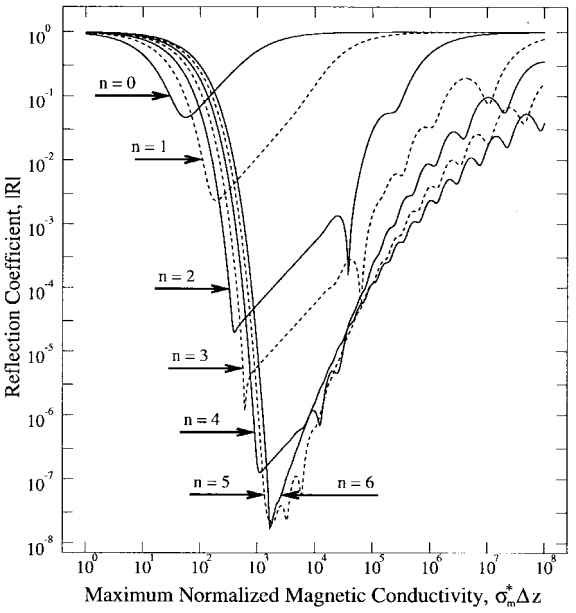

Fig. 7. Reflection from various PML constructions (32) as a function of the maximum normalized magnetic conductivity, $\sigma_m^*\Delta z$. Depth $d = 16\Delta z$, $\lambda/\Delta z = 20$, $\theta = 0°$. (a) polynomial order $n = 0$ constant, (b) $n = 1$ linear, (c) $n = 2$ parabolic, (d) $n = 3$, (e) $n = 4$, (f) $n = 5$, and (g) $n = 6$.

PML conductivity (32), can provide improved performance until around $n = 5$. For $n = 6$, one sees that there is no improvement in the performance of the PML boundary. It is also interesting to note that for the higher order polynomials, the reflection function becomes less smooth for conductivities above the minimum point.

The parabolically graded PML boundaries have received the greatest attention in the literature. Although these PML constructions may not achieve the optimal amount of absorption, this attention may have resulted because of the lack of

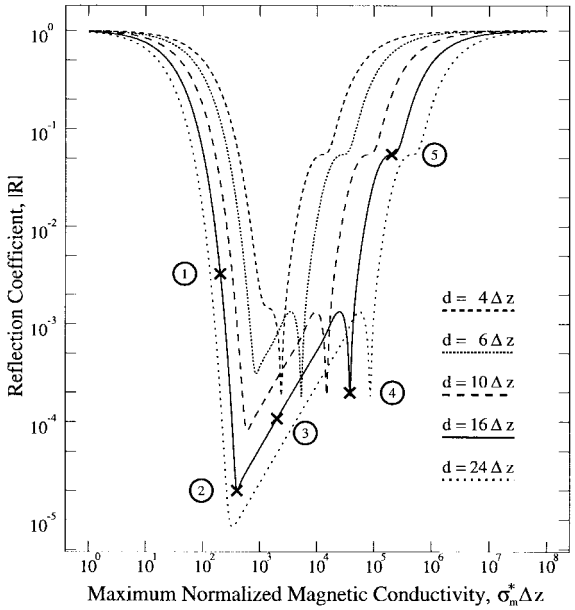

Fig. 8. Reflection from parabolic PML constructions of various depths as a function of the maximum normalized magnetic conductivity. $\lambda/\Delta z = 20$, $\theta = 0°$. (a) depth $d = 4\Delta z$, (b) $d = 6\Delta z$, (c) $d = 10\Delta z$, (d) $d = 16\Delta z$, and (e) $d = 24\Delta z$.

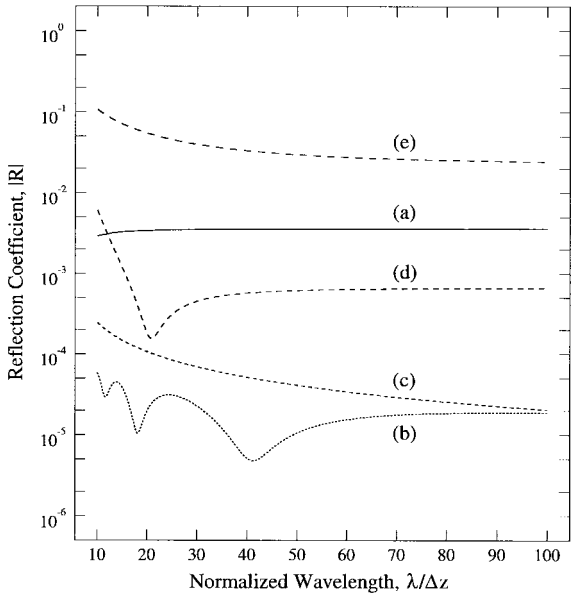

Fig. 9. Reflection from parabolic PML constructions of various maximum conductivity as a function of normalized wavelength. $d = 16\Delta z$, $\theta = 0°$. (a) $\sigma_m^*\Delta z = 200$, (b) $\sigma_m^*\Delta z = 400$, (c) $\sigma_m^*\Delta z = 2 \times 10^3$, (d) $\sigma_m^*\Delta z = 38 \times 10^3$, and (e) $\sigma_m^*\Delta z = 200 \times 10^3$.

any previous accurate analysis method. The following sets of results will concern only the parabolic PML boundaries. The trends evident in the results have been shown to be consistent among all of the polynomial PML constructions (32).

Fig. 8 shows the reflection from a range of parabolic PML absorbing boundaries with varying depth as a function of the maximum conductivity.

As should be expected, the maximum amount of absorption achieved increases with the PML depth. However it is interesting to note that the PML boundaries with the least depth,

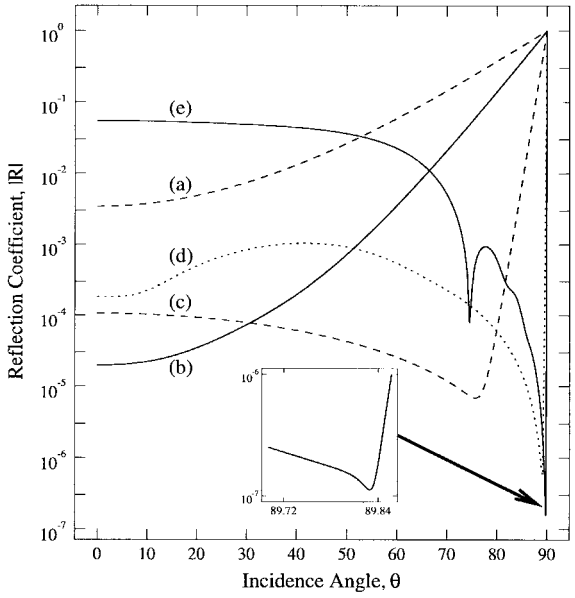

Fig. 10. Reflection from parabolic PML constructions of various maximum conductivity as a function of incidence angle. $d = 16\Delta z$, $\lambda/\Delta z = 20$. (a) $\sigma_m^*\Delta z = 200$, (b) $\sigma_m^*\Delta z = 400$, (c) $\sigma_m^*\Delta z = 2 \times 10^3$, (d) $\sigma_m^*\Delta z = 38 \times 10^3$, and (e) $\sigma_m^*\Delta z = 200 \times 10^3$.

$d = 4\Delta z$ and $d = 6\Delta z$, are able to create a reasonable level of absorption. This is probably a result of the fact that for the shallower PML boundaries, the major factor governing the total absorption is the interference of the reflecting and transmitting waves between the PML layers, and not the actual conductive loss.

A number of points have been marked in Fig. 8, indicating points of interest in the results for a PML of depth $d = 16\Delta z$. These points will be referred to in the following numerical analyses and have been chosen as they represent various choices of maximum conductivity, which result in different PML reflection characteristics.

Fig. 9 shows the reflection from a range of parabolic PML absorbing boundaries with various maximum conductivities as a function of the normalized wavelength. The first observation that one can make is that the reflection functions appear to remain within a range of around 10 dB across most of the spectrum. One can also observe a smooth convergence as the frequency decreases except for the case when the maximum conductivity is at a local minimum ($\sigma_m^*\Delta z = 400$ and $\sigma_m^*\Delta z = 38 \times 10^3$). These points indicate undesirable choices for maximum conductivity.

Fig. 10 shows the reflection from a range of parabolic PML absorbing boundaries with various maximum conductivities as a function of the incidence angle. For the conductivities lower than or equal to the first minimum, $\sigma_m^*\Delta z = 240$ and $\sigma_m^*\Delta z = 400$, the functionality is the same as that predicted by Berenger [1], a gentle rise (logarithmically) to 1. However, after the first minimum, the reflection function assumes a very desirable form; that is, it becomes reasonably constant for a large range of incident angles, assuming almost a step function as grazing incidence is approached. Once again, the choice of conductivity at the other local minima ($\sigma_m^*\Delta z = 38 \times 10^3$) produces an unfavorable response. Above the second

minimum, on the plateau region ($\sigma_m^* \Delta z = 200 \times 10^3$), one can observe an extra element of distortion. These less-smooth responses which occur as the maximum conductivity is increased well above the absolute minimum may influence whether to use higher order polynomial PML boundaries, as they contain an increasing number of the local minima (see Fig. 7).

IV. Conclusion

An in-depth analysis of Berenger's PML boundary truncation technique has been presented. The impedance relationships for the fields within the PML medium have been derived and it has been shown that the impedance of the PML is equal to that of the free-space it surrounds. The dispersion relationship for the fields within the PML medium has also been derived and clearly shows that propagation through the PML medium varies from the propagation in free-space only in the normal direction, where conductive loss occurs.

Some logical points regarding the PML absorbing boundary have been provided to aid in the understanding of how a material with a *perfectly matched* impedance is able to generate a reflection. It is found that there are two mechanisms which contribute toward the total amount of reflection generated from a PML absorbing boundary. These are: 1) reflections between PML/free-space or PML/PML interfaces and 2) the amount of decay experienced as the incident wave travels through the PML medium.

An exact analytical formulation for the calculation of the reflection from an arbitrary PML construction was then developed. Although it was not feasible to compare the algorithm's accuracy to an actual FDTD simulation (due to its accuracy), a range of numerical results was presented. It was found that PML boundaries involving a parabolic increase of the conductivity with depth may not be the best design for PML layering. It was found that the absorptive abilities of the PML boundaries are generally quite stable across a large spectrum of frequencies. Finally, it was found that the range of incident angles for which the polynomial-type PML boundaries are most effective could be maximized by correctly choosing the maximum conductivity.

Acknowledgment

The authors wish to note that while this paper was in preparation it was discovered that Gribbons *et al.* [7] had independently developed a solution for the field dispersion relationship within a PML medium in differential form using a very similar technique to that used to obtain (17).

References

[1] J. P. Berenger, "A perfectly matched layer for the absorption of electromagnetic waves," *J. Comput. Phys.*, vol. 114, pp. 185–200, Aug. 1994.

[2] G. Mur, "Absorbing boundary conditions for the finite-difference approximation of the time-domain electromagnetic-field equations," *IEEE Trans. Electromag. Compat.*, vol. EMC-23, pp. 377–382, Nov. 1981.

[3] J. Fang, "Absorbing boundary conditions applied to model wave propagation in microwave integrated-circuits," *IEEE Trans. Microwave Theory Tech.*, vol. 42, pp. 1506–1513, Aug. 1994.

[4] C. E. Reuter, R. M. Joseph, E. T. Thiele, D. S. Katz, and A. Taflove, "Ultrawideband absorbing boundary condition for termination of waveguiding structures in FD–TD simulations," *IEEE Microwave Guided Wave Lett.*, vol. 4, pp. 344–346, Oct. 1994.

[5] T. G. Jurgens, "A broadband absorbing boundary condition for the FDTD modeling of circular waveguides," in *IEEE MTT-S Int. Symp. Dig.*, Orlando, FL, May 1995, pp. 35–38.

[6] D. S. Katz, E. T. Thiele, and A. Taflove, "Validation and extension to three dimensions of the Berenger PML absorbing boundary condition for FD–TD meshes," *IEEE Microwave Guided Wave Lett.*, vol. 4, pp. 268–270, Aug. 1994.

[7] M. A. Gribbons, W. P. Pinello, and A. C. Cangellaris, "A stretched coordinate technique for numerical absorption of evanescent and propagating waves in planar waveguiding structures," in *IEEE MTT-S Int. Symp. Dig.*, Orlando, FL, May 1995, pp. 31–34.

[8] R. Holland, "Finite-difference solution of Maxwell's equations in generalized nonorthogonal coordinates," *IEEE Trans. Nucl. Sci.*, vol. NS-30, pp. 4589–4591, Dec. 1983.

[9] A. Taflove and K. R. Umashankar, "The finite-difference time-domain method for numerical modeling of electromagnetic wave interactions," *Electromagnetics*, vol. 10, pp. 105–126, 1990.

Deane T. Prescott (S'91–M'97), for a photograph and biography, see this issue, p. 1170.

Nicholas V. Shuley (S'79–M'85), for a photograph and biography, see this issue p. 1170.